Transit Met Chem
DOI 10.1007/s11243-017-0165-5

A one-dimensional Mn(II)-based metal organic oxide: structure and properties

Fa-Nian Shi[1] · Yi-Wen Bai[1] · Miao Lu[1] · C. Cruz[2] · M. S. Reis[2] · Jun Gao[3]

Received: 25 April 2017 / Accepted: 6 July 2017

Abstract A one-dimensional metal organic oxide of Mn(II), with formula $[Mn_3(OH)_2(Hpdc)_2]_n$ (H_3pdc = 3,5-pyrazoledicarboxylic acid), was prepared via the hydrothermal method and its structure solved by single-crystal X-ray diffraction. The compound exhibits a three-dimensional framework structure, comprising three crystallographically unique Mn atoms bridged by OH ligands (O9 and O10) and O atoms from the Hpdc ligands, forming one-dimensional metal–organic oxide chains. Two kinds of magnetic exchange are observed: a strong antiferromagnetic intra-chain interaction, arising from the short distance between Mn(II) centers, and a ferromagnetic inter-chain interaction, due to the larger distances between the chains. The compound shows good photocatalytic activity for the decomposition of methylene blue in aqueous medium under simulated sunlight.

Electronic supplementary material The online version of this article (doi:10.1007/s11243-017-0165-5) contains supplementary material, which is available to authorized users.

✉ Fa-Nian Shi
shifn@sut.edu.cn

[1] School of Science, Shenyang University of Technology, Shenyang 110870, People's Republic of China

[2] Instituto de Física, Universidade Federal Fluminense, Av. Gal. Milton de Souza s/n, Niterói, RJ 24210-346, Brazil

[3] College of Chemical and Environmental Engineering, Shandong University of Science and Technology, Qingdao 266590, People's Republic of China

Introduction

Due to its wide range of accessible oxidation states and easy formation of metal clusters [1], coordination complexes based on manganese have been studied extensively in recent years. These complexes can show very interesting magnetic [2–4] and photoluminescence [5–7] properties. An important question that arises is how to systematically design new structures that possess the target properties. Considering the large number of variables during direct synthesis makes it almost impossible to achieve this goal, an alternative strategy is to approach the synthesis in discrete steps. For example, certain physical properties require metal atoms to be within a certain distance, in order to promote energy transfer and charge transport [8]; on the other hand, when atoms get closer than ca. 5 Å, their electron clouds overlap, resulting in some interesting properties [9–11].

Recently, a new concept of metal–organic oxides (MOO) has been developed as a special class of coordination polymers [12]. In these materials, the distance between adjacent metal centers is within 5 Å (in a similar fashion to inorganic metal oxides). Often, the desired properties may be achieved by designing only the inorganic sub-network via inorganic connectivity, rather than the full material structure [13–17]. In the Mn(II)/3,5-pyrazoledicarboxylic acid system, four related compounds have been described recently [18]. In the present effort, we report another new member, $[Mn_3(OH)_2(Hpdc)_2]_n$ (MOO-Mn1; H_3pdc = 3,5-pyrazoledicarboxylic acid), that we found to consist of 1D inorganic ribbons (triple chains of Mn and O atoms). This compound has mixed ferromagnetic/antiferromagnetic character and interesting photocatalytic properties.

Published online: 14 July 2017

Experimental

The starting chemicals were readily available from commercial sources and used as received without further purification: 3,5-pyrazoledicarboxylic acid monohydrate (H_3pdc, $C_5H_4N_2O_2{\cdot}H_2O$, 97%, Aldrich), manganese powder (Mn, >99.5%, Cymit).

Synthesis of $[Mn_3(OH)_2(Hpdc)_2]_n$

Mn powder (0.0611 g, 1.1121 mmol) and H_3dpc (0.1041 g, 0.7331 mmol) were mixed in distilled water (8.4 g). The mixture was sealed into an autoclave (25 mL), which was placed in a preheated oven at 200 °C for 3 days. Single crystals were harvested by filtration and washed with distilled water (3 × 50 mL) and then air-dried. Yield 0.106 g, ~70% based on H_3dpc.

Anal. Calc. for $Mn_3(OH)_2(Hpdc)_2$ (M = 507.01, %): C, 16.9; H, 1.2; N, 11.0. Found: C, 17.3; H, 2.0; N, 10.9. Selected FTIR bands (Fig. S1, KBr, cm^{-1}): 3615(sh), 3471(br), 1619(s), 1562(s), 1525(s), 1405(s), 1361(s), 1323(s), 1292(m), 1210(m), 1091(w), 1052(m), 1015(m), 845(m), 806(w), 782(m), 636(w), 602(w), 580(w), 536(w), 429(w). TG plot (Fig. 8, weight loss): 178.8–350 °C, −0.4%; 350-502 °C, −54.4%.

Instrumentation

C, N, and H microanalyses were obtained with a Tru-Spec 630-200-200 CNHS Analyzer at the Microanalysis Laboratory at the Department of Chemistry, University of Aveiro. FTIR spectra were collected from KBr pellets (Aldrich 99%+, FTIR grade) on a Mattson 7000 spectrometer in the range of 4000–400 cm^{-1} and a resolution of 2 cm^{-1}. Thermogravimetric analyses (TGA) were carried out using a Shimadzu TGA 50 instrument under air, from room temperature to ca. 700 °C, with a heating rate of 5 °C/min. Powder X-ray diffraction patterns (PXRD) were recorded at room temperature using an Empyrean diffractometer with Cu-Kα radiation (λ = 1.54178 Å) in the 2θ range of 5–50° in transmission mode at 45 kV and 40 mA. Scanning electron microscopy (SEM) and energy-

Table 1 Crystal data and structure refinement for MOO-Mn1

code	MOO-Mn1
formula	$C_{10}H_6Mn_3N_4O_{10}$
Formula weight	507.01
Temperature	180 (2) K
Wavelength	0.71073 Å
Crystal system	Orthorhombic
Space group	*Pna*2(1)
Unit cell dimensions	a = 22.181 (2) Å, α = 90°
	b = 3.3741 (4) Å, β = 90°
	c = 16.9960 (18) Å, γ = 90°
Volume	1272.0 (2) $Å^3$
Z	4
Density (calculated)	2.648 Mg/m^3
F(000)	996
Crystal size	0.12 × 0.04 × 0.02 mm^3
Theta range for data collection	1.84–29.85°
Index ranges	$-28 \le h \le 31$, $-4 \le k \le 4$, $-23 \le l \le 23$
Reflections collected	10,992
Independent reflections	3485 [R(int) = 0.0686]
Completeness to theta = 29.85°	97.3%
Absorption correction	Semiempirical from equivalents
Refinement method	Full-matrix least squares on F^2
Data/restraints/parameters	3485/5/259
Goodness-of-fit on F^2	1.059
Final R indices [I > 2sigma(I)]	$R1$ = 0.0483, $wR2$ = 0.1090
R indices (all data)	$R1$ = 0.0642, $wR2$ = 0.1176
Absolute structure parameter	0.39 (3)
Largest diff. peak and hole	0.587 and −0.864 e.$Å^{-3}$
CCDC No.	1054042

Table 2 Selected bond lengths [Å] and angles [°] for MOO-Mn1

Mn(1)–O(9)#A	2.146(4)	Mn(1)–O(2)	2.152(4)
Mn(1)–O(9)	2.163(4)	Mn(1)–O(8)#B	2.269(4)
Mn(1)–O(8)#C	2.270(4)	Mn(1)–N(2)#D	2.359(5)
Mn(2)–O(9)	2.153(4)	Mn(2)–O(10)	2.158(4)
Mn(2)–O(5)#A	2.275(4)	Mn(2)–O(5)	2.279(4)
Mn(2)–O(1)#E	2.292(4)	Mn(2)–O(1)	2.297(4)
Mn(3)–O(10)	2.136(4)	Mn(3)–O(4)#F	2.183(4)
Mn(3)–O(6)	2.194(4)	Mn(3)–O(10)#E	2.212(4)
Mn(3)–N(4)#G	2.344(5)	Mn(3)–O(4)#H	2.400(4)
Mn(1)–Mn(1)′	3.3741(10)	Mn(2)–Mn(2)′	3.3741(10)
Mn(3)–Mn(3)′	3.3741(10)	Mn(1)–Mn(2)	3.6877(12)
Mn(1)–Mn(3)	3.6576(13)	N(1)–N(2)	1.334(7)
N(3)–N(4)	1.330(7)	O(2)–Mn(1)–O(9)	91.42(16)
O(2)–Mn(1)–O(8)#B	84.09(15)	O(9)–Mn(1)–O(8)#B	174.39(16)
O(2)–Mn(1)–N(2)#D	168.32(16)	O(9)–Mn(1)–N(2)#D	95.54(15)
O(9)–Mn(2)–O(10)	171.47(14)	O(9)–Mn(2)–O(5)	92.00(15)
O(10)–Mn(2)–O(5)	93.94(14)	O(5)#A–Mn(2)–O(5)	95.62(15)
O(9)–Mn(2)–O(1)	87.43(14)	O(10)–Mn(2)–O(1)	86.68(15)
O(5)-Mn(2)–O(1)	179.22(16)	O(1)#E–Mn(2)–O(1)	94.64(16)
O(10)–Mn(3)–O(6)	86.63(16)	O(4)#F–Mn(3)–O(6)	84.46(15)
O(10)–Mn(3)–O(10)#E	101.80(17)	O(10)–Mn(3)–N(4)#G	95.28(16)
O(6)–Mn(3)–N(4)#G	161.37(16)	O(10)–Mn(3)–O(4)#H	79.46(14)
Mn(2)#A–O(1)–Mn(2)	94.64(16)	Mn(3)#C–O(4)–Mn(3)#B	94.70(15)
Mn(2)#E–O(5)–Mn(2)	95.62(15)	Mn(1)#H–O(8)–Mn(1)#F	96.03(16)
Mn(1)#E–O(9)–Mn(2)	118.13(18)	Mn(1)#E–O(9)–Mn(1)	103.09(17)
Mn(2)–O(9)–Mn(1)	122.21(19)	Mn(3)–O(10)–Mn(2)	116.80(18)
Mn(3)–O(10)–Mn(3)#A	101.79(17)	Mn(2)–O(10)–Mn(3)#A	126.71(18)

Symmetry transformations used to generate equivalent atoms:

#A x,y+1,z; #B x-1/2,-y+3/2,z; #C x-1/2,-y+1/2,z; #D -x,-y+2,z-1/2; #E x,y-1,z; #F x+1/2,-y+1/2,z; #G -x+1/2,y+1/2,z+1/2; #H x+1/2,-y+3/2,z; #I -x,-y+2,z+1/2; #J -x+1/2,y-1/2,z-1/2.

Table 3 Hydrogen bonds for MOO-Mn1 [Å and °]

D-H…A	d(D-H)	d(H…A)	d(D…A)	<(DHA)
N(1)–H(1 N)…O(7)#11	0.85(2)	1.84(3)	2.642(6)	155(6)
N(3)–H(3 N)…O(3)#12	0.86(2)	2.26(11)	2.698(6)	112(9)
O(9)–H(9)…O(3)#13	0.82(2)	1.86(2)	2.674(5)	169(7)
O(10)–H(10)…O(7)#11	0.81(2)	2.17(5)	2.775(6)	131(6)

Symmetry transformations used to generate equivalent atoms:

#11 -x+1/2,y+3/2,z+1/2; #12 -x,-y,z-1/2; #13 -x,-y+1,z-1/2.

dispersive analysis of X-ray spectroscopy (EDS) were performed using a scanning electron microscope S4100 working at 25 kV, with the working distance maintained at 15 mm. Samples were prepared by deposition on aluminum sample holders followed by carbon coating. EDS results collected on several different particles confirmed the presence of manganese in the single crystals.

Single-crystal X-ray diffraction

Single-crystal X-ray diffraction data collection was performed on a Bruker Apex II CCD diffractometer operating at 50 kV and 30 mA using Mo Kα radiation ($\lambda = 0.71073$ Å) at 180 K. Data collection and reduction were performed using the SMART and SAINT software packages [19]. A multi-scan absorption correction was applied using the SADABS program [20]. The structure was solved by direct methods [21] and refined by full-matrix least squares on F^2 using the SHELXTL program package [22]. All non-hydrogen atoms were refined anisotropically. C-bound H atoms were geometrically positioned and allowed to ride on their parent atoms and

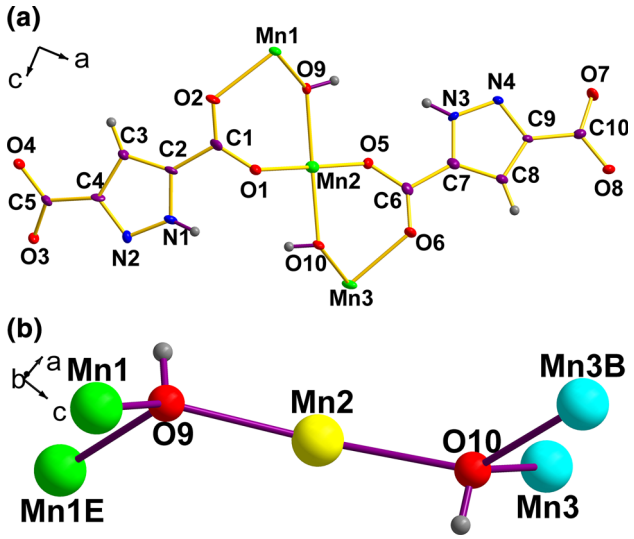

Fig. 1 **a** Schematic representation of the asymmetric unit of MOO-Mn1 with thermal ellipsoids drawn at the 50% probability level and hydrogen atoms represented as small spheres of an arbitrary radius. A labeling scheme is provided for all non-hydrogen atoms. **b** *Ball* and *stick* representation of the coordination environments of O9 and O10 atoms. The symmetry codes are as given in Table 2: #B x-1/2,-y+3/2,z; #E x,y-1,z

refined isotropically. Hydrogen atoms bonded to nitrogen and oxygen atoms were located from difference Fourier maps and isotropically refined with the N–H and O–H distances restrained to 0.85 and 0.82 Å, respectively; Uiso values were set to 1.2 Ueq (parent atom) for these H atoms. PLATON was used for the cif file check, and DIAMOND for molecular graphics. Detailed crystallographic data are given in Table 1, selected bond lengths and angles in Table 2, and hydrogen bonds parameters in Table 3.

Magnetic measurements

Magnetic susceptibility was acquired as a function of temperature (4–300 K) at 200 Oe using a commercial Superconducting Quantum Interference Device (SQUID magnetometer from Quantum Design®) at the Instituto de Física Gleb Wataghin, UNICAMP (Campinas, Brazil).

Photocatalytic experiments

The photocatalytic activity of MOO-Mn1 was assessed by the degradation of methylene blue (MB) in aqueous medium. A solution of MB in water with a concentration of 20 mg L^{-1} (100 mL aqueous solution) was mixed with 0.0526 mg of the test compound and exposed to simulated solar light (wavelength = 320–2500 nm). Before turning on the lamp, the suspension containing MB and the photocatalyst was magnetically stirred in the dark for 30 min to reach adsorption–desorption equilibrium. A 3-mL aliquot of the suspension was removed from the reactor and centrifuged immediately to separate the suspended solid. The lamp was then turned on, and further aliquots were collected every 30 min until the absorbance approached zero or no further change in the color of the solution was observed. The absorbance of the transparent solution was

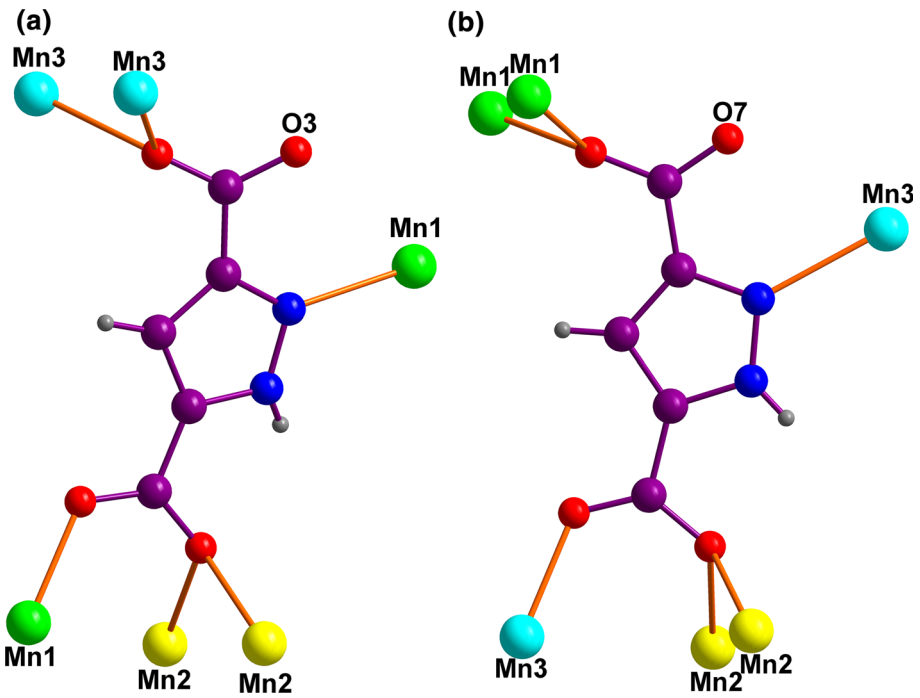

Fig. 2 Two unique coordination modes of the pdc ligand in $[Mn_3(OH)_2(Hpdc)_2]_n$. **a** $d_{Mn1–O3}$ = 3.4954(39) Å; **b** $d_{Mn3–O7}$ = 3.0074(40) Å

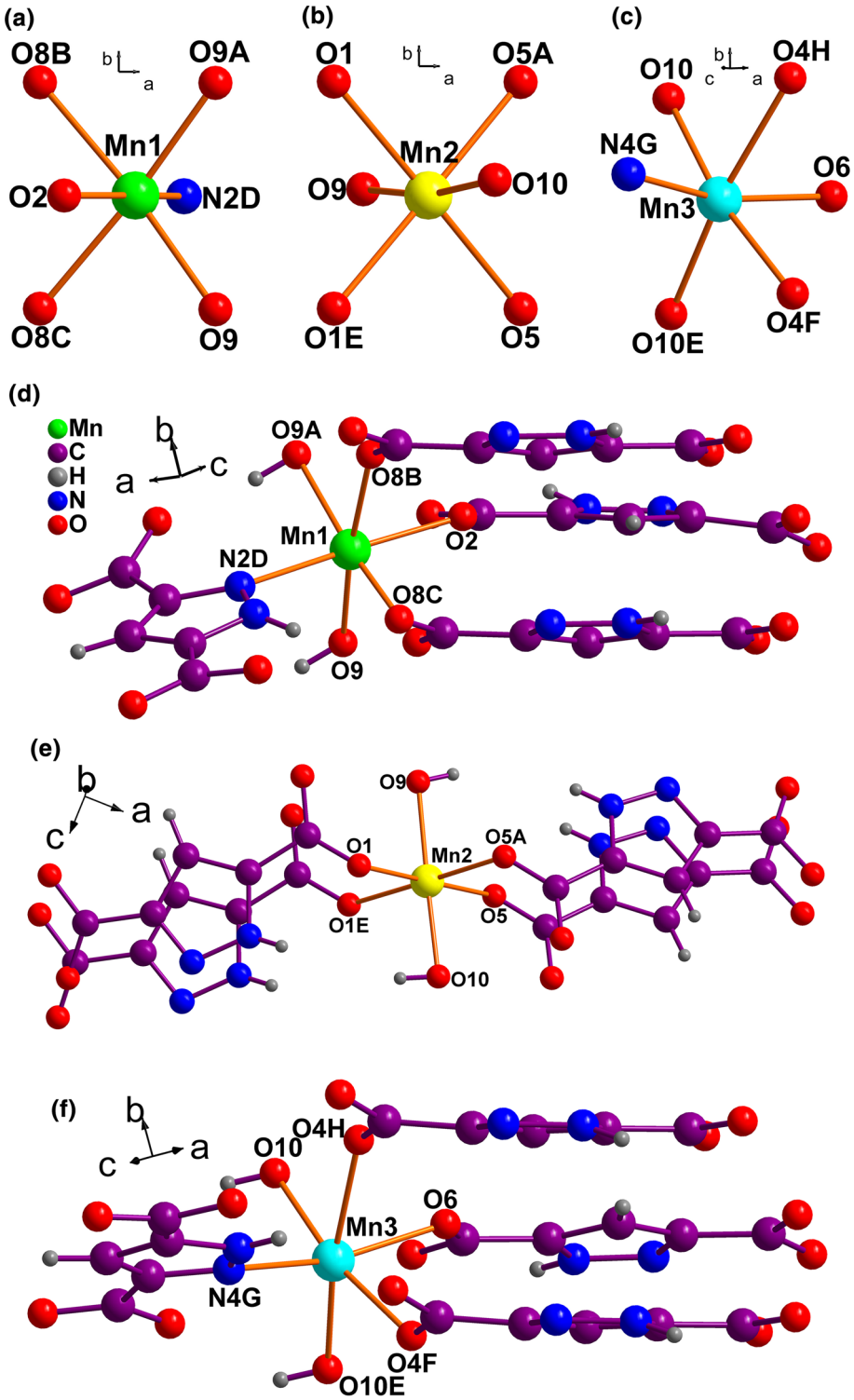

Fig. 3 Coordination environment of **a** Mn1, **b** Mn2 and **c** Mn3. **d** Two O9 atoms and four Hpdc ligands bind to Mn1. **e** One O9, one O10, and four Hpdc ligand bind to Mn2. **f** Two O10 atoms and four Hpdc ligand bind to Mn3. The symmetry codes are as given in Table 2: #A x,y+1,z; #B x-1/2,-y+3/2,z; #C x-1/2,-y+1/2,z; #D -x,-y+2,z-1/2; #E x,y-1,z; #F x+1/2,-y+1/2,z; #G -x+1/2,y+1/2,z+1/2; #H x+1/2,-y+3/2,z

analyzed on a UV–visible spectrophotometer. After the first cycle, the photocatalyst was retrieved by centrifugal separation, washed with distilled water, and dried under ambient conditions. The recovered photocatalyst used for the second cycle was only 0.006 g, with a similar process to the first cycle.

Results and discussion

Structure description

MOO-Mn1 crystallizes in orthorhombic symmetry and *Pna*2(1) space group (Table 1). The asymmetric unit

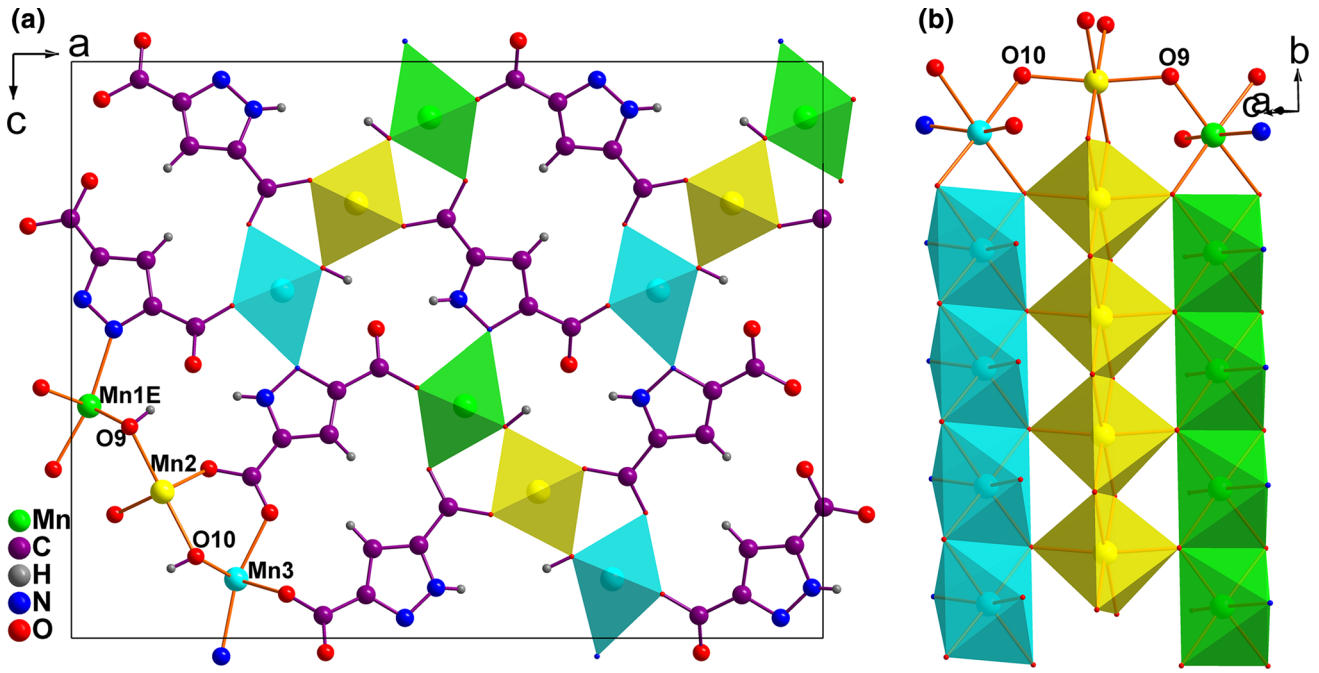

Fig. 4 **a** Polyhedron view of the unit cell of $[Mn_3(OH)_2(Hpdc)_2]_n$ viewed along the *b* axis. **b** Infinite oxide ribbon along the *b* axis with short Mn–Mn contacts. $d_{Mn1–Mn1} = d_{Mn2–Mn2} = d_{Mn3–Mn3} = 3.3741$ (10) Å, $d_{Mn1–Mn2} = 3.6877$ (12) Å and 3.7792 (12) Å, $d_{Mn3–Mn2} = 3.6576$ (13) Å and 3.9062 (12) Å as depicted in Table 2. In (**b**), C and H atoms are omitted for clarity

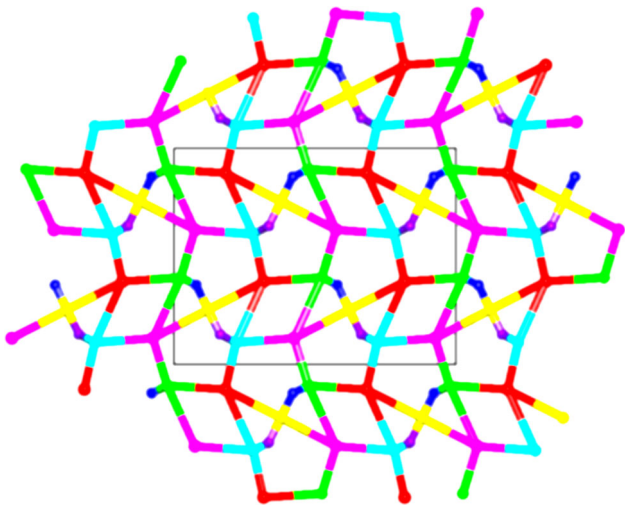

Fig. 5 Topological representation of MOO-Mn1 along the *b* axis as a hepta-nodal 3,3,6,6,6,6,6-connected network with a total point symbol $\{4^3\}_2\{4^7.6^8\}_2\{4^8.6^6.8\}_3$. Nodes: Mn1 cation; Mn2 cation; Mn3 cation; and two different oxygen atoms (O9 and O10); and centers of gravity of two different $Hpdc^{2-}$

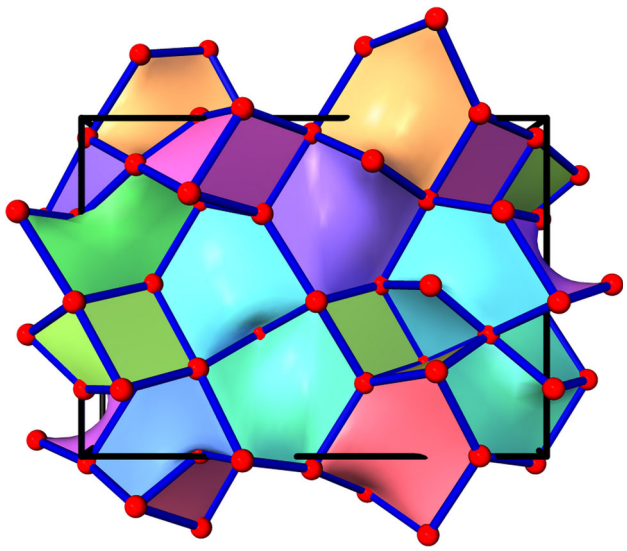

Fig. 6 Natural tiling of 3-periodic net in MOO-Mn1

comprises three unique Mn^{2+} centers (Mn1, Mn2, and Mn3), two independent Hpdc ligand fragments and two hydroxyl groups (O9 and O10), as shown in Fig. 1a. The latter are important for forming a one-dimensional MOO because they are directly bonded to five metal centers (Fig. 1b) and serve as suitable bridging ligands, with bond distances ranging from 2.136(4) Å (Mn3–O10) to 2.211(4) Å (Mn3B–O10, Table 2). The Hpdc ligand connects the metal centers in a flexible way, as indicated by the wide gamut of bond lengths, from 2.153(4) Å (Mn1–O2) to 2.401(4) Å (Mn3–O4H, Table 2). These values are in the ranges observed for $Mn_4(H_2O)_6(Hpdc)(pdc)_2{\cdot}H_2O$ [18] and $[Mn_2(oba)_2(2,2'\text{-bpy})_2(H_2O)_2]_n{\cdot}nH_2oba$ [23]. The Hpdc coordination modes are unusual (Fig. 2); in particular, the N atoms coordinate to Mn (Mn1 and Mn3) without chelation from the carboxylate oxygens, although O3 and

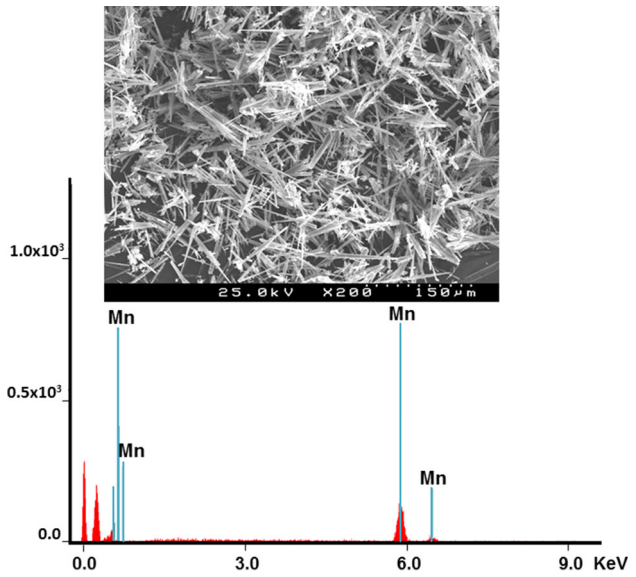

Fig. 7 (*Top*) SEM image of MOO-Mn1 showing a needle-like crystal habit; (*Bottom*) EDS spectrum indicating the presence of Mn in the crystals

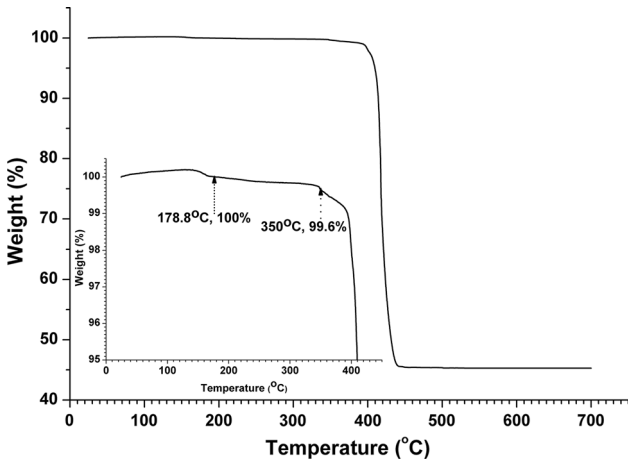

Fig. 8 TGA curve of MOO-Mn1 measured from room temperature to 700 °C, in air. The *inset* shows the first step of weight loss attributed to the removal of H atoms from hydroxyl groups and release of H_2O molecules

O7 are free ($d_{O–Mn} > 3.00$ Å). This phenomenon was previously observed in only two other compounds [24, 25].

All of the Mn atoms in MOO-Mn1 are six-coordinated (Fig. 3a–c) in slightly distorted octahedra. Mn1 is coordinated to three carboxylate oxygen atoms (O2, O8B, O8C) from three Hpdc fragments, one nitrogen atom (N2D) from another Hpdc ligand and two oxygen atoms (O9, O9A) from hydroxyl ligands (Fig. 3d). Mn2 links to four carboxylate oxygen atoms (O1, O1E, O5, O5A) from four Hpdc fragments and two hydroxyl oxygen atoms (O9, O10) (Fig. 3e). Mn3 coordinates to three carboxylate oxygen atoms (O6, O4F, O4H) from three Hpdc fragments, one nitrogen atom (N4G) from another Hpdc moiety and two hydroxyl oxygen atoms (O10, O10E) (Fig. 3f). These connections result in a dense three-dimensional framework (Fig. 4a), whose main feature is the one-dimensional MOO ribbons (Fig. 4b) formed by the O9 and O10 atoms linking Mn1, Mn2 and Mn3 chains, resulting in short metal–metal distances (Table 2 and Fig. 4: 3.3741(10)–3.9062(12) Å) inside the oxide ribbon. The observed magnetic properties are derived directly from this structural feature. There are strong hydrogen bonding interactions which occur between OH groups (O9 and O10), protonated N atoms (N1 and N3), and non-bonded O3 and O7 atoms (Table 3 and Fig. S3).

The topology of this framework was analyzed using the TOPOS program [26] with simplified standard methodology. The three metal centers, two different Hpdc fragments, and two O atoms (O9 and O10) were treated as unique nodes. The three-dimensional net is a hepta-nodal 3,3,6,6,6,6,6-connected network with a total point symbol $\{4^3\}_2\{4^7.6^8\}_2\{4^8.6^6.8\}_3$, which is an unprecedented topological type (Fig. 5). The tiling was also analyzed with TOPOS (Fig. 6 shows one natural tiling). There are 7, 18, 22, and 11 inequivalent vertices, edges, faces, and tiles in the natural tiling, respectively. The 22 faces are composed of 11 essential 4-membered rings (4a-4 k) and 11 essential 6-membered rings (6b,6d,6e,6 g,6j,6 k,6 l,6n,6o,6r,6 s; Fig. 6). The 11 kinds of tiles (Fig. 6 in 11 different colors) correspond to $2[4.6^2]$, $2[6^3]$, $3[4^2.6^2]$, $2[4.6^3]$, $2[4^6]$ with the intricate transitivity of [7(18)(22)(11)].

SEM, FTIR, powder XRD, and TGA

SEM shows that the crystals exhibit a needle-like habit (Fig. 7) and confirms their phase purity, while EDS analysis (point method) on the several needle-like particles indicates the presence of Mn. The FTIR spectrum (Experimental section and Fig. S1) displays several strong peaks, at 1619, 1562, 1525, 1405, 1361, and 1323 cm^{-1}, assigned to the asymmetric and symmetric stretching vibrations of the coordinated carboxylate groups [15, 18], which suggests that all the carboxylic groups of the pdc ligand have been deprotonated and coordinated to the metal atoms, consistent with the crystal structure. The powder XRD pattern (Fig. S2) is also consistent with the single-crystal structure, indicating that the bulk phase is identical to the single-crystal structure.

The TGA curved was measured in air with a heating rate of 5 °C/min. Over the whole temperature range, the weight loss can be divided into two stages. The first stage (Fig. 8, inset) occurs in the region of 178.8–350 °C with a weight loss of ca. 0.4%, corresponding to removal of the H atoms from bonded hydroxyl groups (calculated 0.39%),with

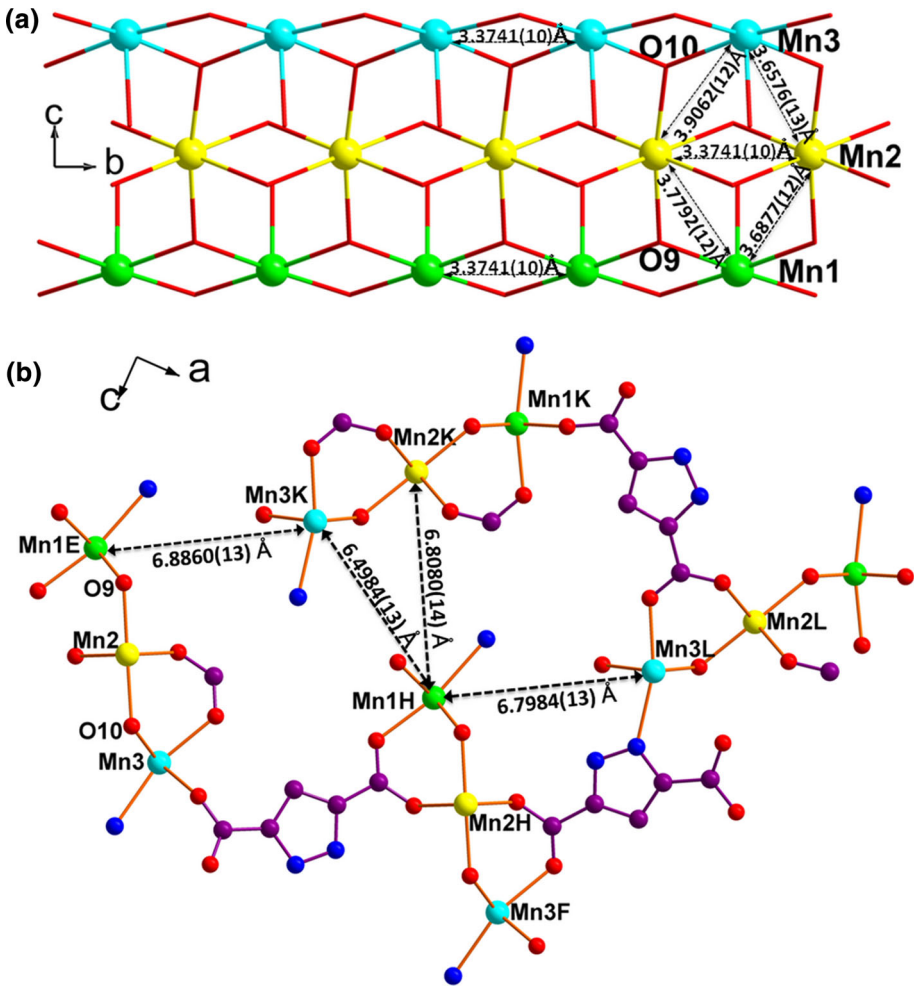

Fig. 9 **a** Metal distances within the triple chain; **b** distances between the triple chains in MOO-Mn1 derived from the single-crystal structure (*red*, *blue,* and *purple balls* are oxygen, nitrogen, and carbon atoms, respectively; hydrogen atoms are omitted for clarity.). The symmetry codes in (**b**) E: x, −1 + y, z; F: 0.5 + x, 0.5-y, z; H: 0.5 + x, 1.5-y, z; K: 0.5-x, −0.5 + y, −0.5 + z; L: 1-x, 1-y, −0.5 + z. (Color figure online)

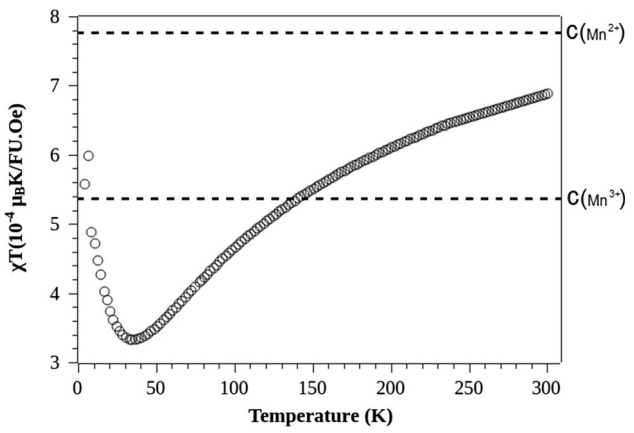

Fig. 10 Plot of χT as function of temperature. *Dashed lines* indicate the Curie constants (C) of Mn (II) and Mn (III)

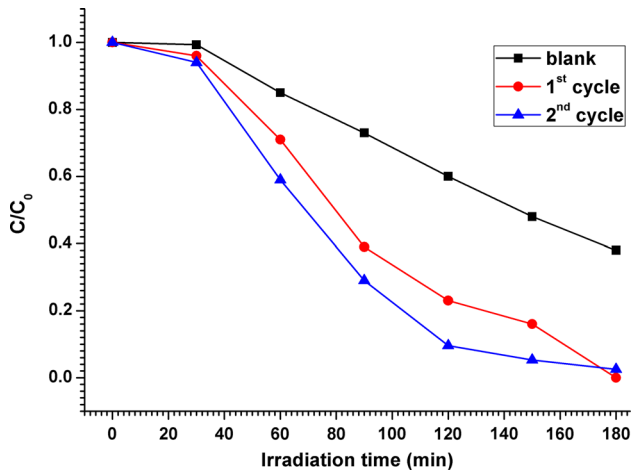

Fig. 11 Concentration of MB as a function of irradiation time, under the simulated solar light with MOO-Mn1 as photocatalyst, plus a blank experiment without any photocatalyst

concomitant oxidation of Mn(II) to Mn(III). This process is rationally explained by the redox reaction shown in Eq. (1). The second stage takes place between 350 and 502 °C with a weight loss of 54.4%, due to the decomposition of pdc ligand and formation of Mn_3O_4 (calculated 54.9%). PXRD measurement shows that the residue is

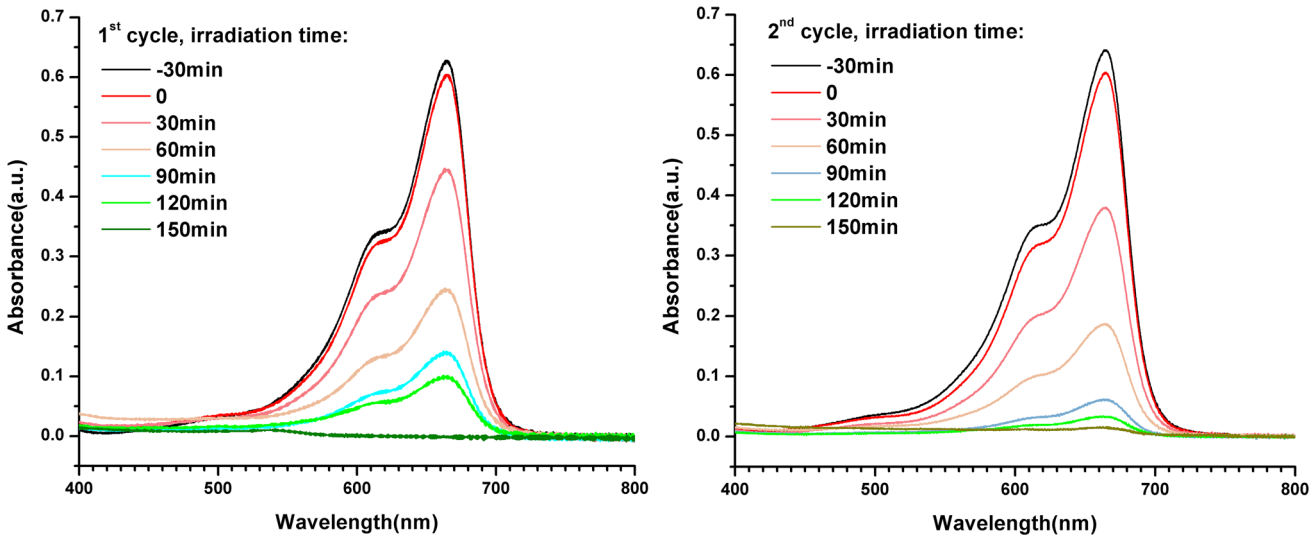

Fig. 12 Curves of UV–Vis spectra for the first and second cycles experiments with different illumination time showing MB was effectively degraded by MOO-Mn1 in aqueous medium under simulated sunlight. Only *red curve* was the indication of MB aqueous solution stirred in the dark with presence of MOO-Mn1 as photocatalyst. (Color figure online)

amorphous, which is also consistent with reported amorphous Mn_3O_4 [27].

$$6OH^- + O_2 + 4Mn^{2+} = 4Mn^{3+} + 5O^{2-} + 3H_2O \quad (1)$$

Magnetic properties

In MOO-Mn1, the manganese(II) centers are connected by *d-p-d* bounds forming triple chains, separated from each other by ca. 7 Å (Fig. 9). The χT data (Fig. 10) are quite far from the Curie constant, and this is a clear signature that the exchange interactions are strong, even at room temperature. In other words, the magnetic energy is larger than the room temperature thermal energy. Thus, the paramagnetic regime is not achieved until 300 K and the compound cannot be described by the Curie–Weiss law in this temperature range (4–300 K).

Two χT regimes may be considered as follows. Above 35 K, this quantity steadily increases with increasing temperature, a behavior usually associated with antiferromagnetic low-dimensional systems [28, 29], due to strong negative intra-chain interactions resulting from the short distance between the Mn(II) centers. Below 35 K, χT increases with decreasing temperature, a behavior attributed to the onset of ferromagnetic inter-chain interactions. The valence of the manganese atoms can be obtained from the χT plot, and for this purpose Fig. 10 depicts two dashed lines representing the Curie constants of the Mn(II) and Mn(III) ions. Clearly, at high temperature, χT tends to the Curie constant of Mn(II), in accordance with previous reports on systems with Mn(II) ions in octahedral symmetry [30, 31].

Photocatalytic studies

Sunlight is a powerful resource for photocatalysis [32–35]. TiO_2 and its composites are the most studied photocatalysts for the degradation of methylene blue (MB) under illumination [36–39]. To date, few studies have reported on the use of Mn-based coordination polymers to photocatalyze MB degradation [40]. Therefore, MOO-Mn1 was used as a photocatalyst to degrade MB at room temperature with simulated solar light irradiation. Under ambient conditions, MOO-Mn1 is not soluble in water and many common organic solvents including ethanol, acetone, phenol, DMF, and DMSO. A blank experiment (no added photocatalyst) plus two cycles of photocatalysis were performed under similar conditions; the only difference between the first and second cycles was the addition of different quantities of MOO-Mn1 as photocatalyst. For the first cycle, 0.0526 g of the photocatalyst was added and for the second cycle, 0.006 g of the photocatalyst was added (which was retrieved from the first cycle). The photocatalytic properties were monitored by observing the change in the maximum absorbance at $\lambda = 664$ nm, to determine the residual concentration of MB in solution. The degradation efficiencies of MB in the presence of MOO-Mn1 and in the absence of MOO-Mn1 (blank experiment) after pre-equilibration in the dark for 30 min are depicted in Fig. 11, and the degradation curves of MB for the first and the second cycles are shown in Fig. 12. The degradation efficiency of MB increased from 62.2% (blank experiment) to 100 and 97.3% for the first and second cycles, respectively, after 3 h. Compared to those Mn-based complexes already described in the literature [40–45], MOO-Mn1 showed

average catalytic activity in this reaction. Hence, MOO-Mn1 effectively photocatalyzes the degradation of MB in aqueous solution under simulated sunlight, and the photocatalyst can be recovered and reused with good efficiency, although it appears to slowly dissolve into aqueous solution during these experiments.

Conclusions

In summary, a 1-D MOO material with formula $Mn_3(OH)_2(Hpdc)_2$ has been prepared via the hydrothermal method. The three-dimensional framework includes three unique Mn(II) centers and features infinite MOO triple chains built up through the hydroxyl groups linking the metal atoms. MOO-Mn1 has an unusual topology type, and its magnetic properties cannot be explained by the Curie–Weiss law. Two magnetic exchange interactions were rationalized on the basis of the crystal structure: a strong antiferromagnetic interaction between the Mn(II) ions within the triple chains, and a ferromagnetic interaction between the triple chains. MOO-Mn1 is an interesting photocatalyst, being capable of the degradation of MB in aqueous medium under simulated sunlight.

Acknowledgements We acknowledge the National Natural Science Foundation of China (Grant No: 21571132). The authors thank Adelino Aguiar, from UNICAMP, Brazil for the magnetic measurements.

References

1. Kostakis GE, Akoa AM, Powell AK (2010) Chem Soc Rev 39:2238–2271
2. Lymperopoulou S, Papastergiou M, Louloudi M, Raptopoulou CP, Psycharis V, Milios CJ, Plakatouras JC (2014) Eur J Inorg Chem 2014:3638–3644
3. Sutradhar M, Martins LMDRS, Guedes da Silva MFC, Alegria ECBA, Liu C-M, Pombeiro AJL (2014) Dalton Trans 43:3966–3977
4. Wu L-F, Wang Z-X, Geng J-P, Xiao H-P, Li M-X (2014) Inorg Chim Acta 412:1–5
5. Nath JK, Mondal A, Powell AK, Baruah JB (2014) Cryst Growth Des 14:4735–4748
6. Alexandropoulos DI, Mowson AM, Pilkington M, Bekiari V, Christou G, Stamatatos TC (2014) Dalton Trans 43:1965–1969
7. Zhang L-P, Zhu L-G (2006) CrystEngComm 8:815–826
8. Allendorf MD, Schwartzberg A, Stavila V, Talin AA (2011) Chem Eur J 17:11372–11388
9. Chen XF, Zang H, Wang X, Cheng JG, Zhao RS, Cheng CG, Lu XQ (2012) Analyst 137:5411–5419
10. Cheng JY, Wang P, Ma JP, Liu QK, Dong YB (2014) Chem Commun 50:13672–13675
11. Huang YQ, Wang YH, Zhao Y, Zhao Q, Yang Y, Zhao W, Shao Q (2013) Inorg Chim Acta 394:164–170
12. Shi F-N, Rosa Silva A, Bian L (2015) J Solid State Chem 225:45–52
13. Liu CB, Ferreira RAS, Almeida Paz FA, Cadiau A, Carlos LD, Fu LS, Rocha J, Shi F-N (2012) Chem Commun 48:7964–7966
14. Yang T-H, Rosa Silva A, Shi F-N (2013) Dalton Trans 42:13997–14005
15. Shi F-N, Rosa Silva A, Yang T-H, Rocha J (2013) CrystEngComm 15:3776–3779
16. Antonio de Campos E, Silva NJO, Shi F-N, Rocha J (2014) CrystEngComm 16:10439–10444
17. Yang T-H, Ferreira RAS, Carlos LD, Rocha J, Shi F-N (2014) RSC Adv 4:7818–7825
18. Shi F-N, Yang T-H (2014) Inorg Chim Acta 412:79–87
19. Bruker (2004) APEXII software, version 6.3.1. Bruker AXS Inc., Madison
20. Sheldrick GM (1996) SADABS program for scaling and correction of area detector data. University of Göttingen, Göttingen
21. Sheldrick GM (1997) SHELXS-97, program for X-ray crystal structure refinement. University of Göttingen, Göttingen
22. Sheldrick GM (1997) SHELXL-97, program for X-ray crystal structure refinement. University of Göttingen, Göttingen
23. Sun C-Y, Gao S, Jin L-P (2006) Eur J Inorg Chem 2006:2411–2421
24. Yang J-H, Zheng S-L, Yu X-L, Chen X-M (2004) Cryst Growth Des 4:831–836
25. Pan L, Huang XY, Li J (2000) J Solid State Chem 152:236–246
26. Blatov VA, Shevchenko AP, Proserpio DM (2014) Cryst Growth Des 14:3576–3586
27. Hu C-C, Hung C-Y, Chang K-H, Yang Y-L (2011) J Power Sources 196:847–850
28. Brandão P, Reis MS, Gai Z, dos Santos AM (2013) J Solid State Chem 198:39–44
29. Brandão P, Rocha J, Reis MS, dos Santos AM, Jin R (2009) J Solid State Chem 182:253
30. Esteves D, Tedesco JCD, Pedro SS, Cruz C, Reis MS, Brandão P (2014) Mater Chem Phys 147:611–616
31. Shi F-N, Reis MS, Brandão P, Souza AM, Felix V, Rocha J (2010) Trans Met Chem 35:779–786
32. Guo WF, Li HP, Ma HS, Teng WX (2014) J Chem 2014:1–5
33. Reddy PR, Shireesha V, Malapat V, Venkateswara Rao K, Aparna Y (2015) Int J Eng Adv Technol 4:146–151
34. Abdelhameed RM, Simões MMQ, Silva AMS, Rocha J (2015) Chem Eur J 21:11072–11081
35. Zhang XY, Ge SS, Shao Q, Liu M, Liu QY (2016) Chin J Inorg Chem 32:1535–1542
36. Wei N, Cui HZ, Song Q, Zhang LQ, Song XJ (2016) Appl Catal B Environ 198:83–90
37. Houas A, Lachheb H, Ksibi M, Elaloui E, Guillard C, Herrmann J-M (2001) Appl Catal B Environ 31:145–157
38. Yao W, Zhang B, Huang C, Ma C, Song X, Xu Q (2012) J Mater Chem 22:4050–4055
39. Xiao Q, Zhang J, Xiao C, Tan X (2008) Catal Commun 9:1247–1253
40. Wang C-C, Gao F, Guo X-X, Jing H-P, Wang P, Gao S-J (2016) Transit Met Chem 41:375–385
41. Li YL, Zhao Y, Kang Y-S, Liu X-H, Sun W-Y (2016) Cryst Growth Des 16(12):7112–7123
42. Hao X-L, Jia S-F, Ma Y-Y, Wang H-Y, Li Y-G (2016) Inorg Chem Commun 72:132–137
43. Zhou Y, Yang W, Qin M, Zhao H (2016) Appl Organomet Chem 30:188–192
44. Wang C-C, Zhang Y-Q, Zhu T, Zhang X-Y, Wang P, Gao S-J (2015) Polyhedron 90:58–68
45. Zhang J, Wang C-C (2017) J Mol Struct 1130(15):223–230